

# High-entropy Advantage in Neural Networks' Generalizability

Entao Yang<sup>1</sup>, Xiaotian Zhang<sup>2</sup>, Yue Shang<sup>2, 3</sup>, and Ge Zhang<sup>2, \*</sup>

<sup>1</sup>Innovation Campus Delaware, Air Liquide, Newark, DE, USA

<sup>2</sup>Department of Physics, City University of Hong Kong, Hong Kong, China

<sup>3</sup>Department of Physics, University of Science and Technology of China, Hefei, China

\*e-mail: gzhang37@cityu.edu.hk

## ABSTRACT

While the 2024 Nobel Prize in Physics ignites a worldwide discussion on the origins of neural networks and their foundational links to physics, modern machine learning research predominantly focuses on computational and algorithmic advancements, overlooking a picture of physics. Here we introduce the concept of entropy into neural networks by reconceptualizing them as hypothetical physical systems where each parameter is a non-interacting 'particle' within a one-dimensional space. By employing a Wang-Landau algorithm, we construct the neural networks' (with up to 1 million parameters) entropy landscapes as functions of training loss and test accuracy (or loss) across four distinct machine learning tasks, including arithmetic question, real-world tabular data, image recognition, and language modeling. Our results reveal the existence of *entropy advantage*, where the high-entropy states generally outperform the states reached via classical training optimizer like stochastic gradient descent. We also find this advantage is more pronounced in narrower networks, indicating a need of different training optimizers tailored to different sizes of neural networks.

## Main

### Intro

Neural Networks (NNs) have shown remarkable success in solving a wide range of machine learning problems, from image recognition to natural-language processing.<sup>1-4</sup> Despite their success, applications can face the problem of overfitting<sup>5-8</sup>, which occurs when an NN learns not only the underlying patterns in the training data, but also the noise and random fluctuations. Consequently, the NN could perform exceptionally well on the training data but fail to generalize to new, unseen data. The ability to generalize is a critical metric to evaluate their usefulness in the real-world applications, making *generalizability* one of the central topics in the field.<sup>6,8,9</sup> Modern NNs are usually overparameterized, i.e., the number of parameters exceeds the number of training data points.<sup>10,11</sup> Intuitively, an overparameterized model can easily overfit the training data, akin to how a high-order polynomial fit generally fails to capture the underlying trend of the data. In fact, today's NNs have sufficient capacity to memorize the entire training set, as evidenced by their ability to easily fit data with random labels.<sup>6</sup> However, despite their massive size, NNs have achieved state-of-art generalization performance in many different machine-learning tasks.<sup>12-14</sup> Such surprising generalization has sparked extensive research to understand its underlying mechanism.

Analogous to the representation of all degrees of freedom in a physical system as a point in high-dimensional phase space, all trainable parameters in a neural network can likewise be depicted as a point in a similarly high-dimensional parameter space. For an over-parameterized neural network, there are infinitely many points in the parameter space that can perfectly fit the training data. Some of the points generalize well, while others do not. Therefore, many studies on generalizability looked for its correlation with certain characteristics in the parameter space, including sharpness, the VC dimension, Rademacher complexity, weight norms, and intrinsic dimension<sup>15-18</sup>. Unfortunately, this line of research has not yet generated convincing conclusions,<sup>16</sup> as the best-performed measure, sharpness, has been challenged to be sufficient enough to determine the generalization by itself.<sup>19,20</sup> There are also studies attributing the generalizability to different regularization methods,<sup>5,6,21,22</sup> which are protocols that bias the training trajectory toward some specific parts of the parameter space that have been empirically found to generalize well. Although empirical studies suggest that regularization can help generalization, many modern NNs can still generalize well without these methods, excluding them as the fundamental mechanism of generalization.<sup>6</sup>

Here we investigate the mystery of NN generalizability from a physics perspective and show that among all states that fits the training data well, the highest-entropy ones are highly generalizable. Since entropy is the logarithm of the parameter-space volume, our results demonstrate that generalizable well-trained states occupy a *larger* part of the parameter space than its non-generalizable analog. This explains why training algorithms can find generalizable states, even when we do not actively

apply regularization methods. In fact, our results show that max entropy states often generalize even better than states trained with stochastic gradient descent (SGD). In other words, SGD usually biases toward slightly less generalizable parameters, but the generalizable part of the parameter space is so massive that SGD-trained states can generalize well anyway. We intentionally choose to compare with SGD training rather than other popular optimizers like Adam, because it has been shown previously that SGD can usually realize better generalization in neural networks training.<sup>23–25</sup> We examined the entropy-generalizability relations in four distinct machine learning tasks, including arithmetic question, real-world tabular data, image recognition, and language modeling. Our results demonstrate that in all four tasks, the generalizability of high-entropy states are better or at least comparable with the states reached via the classical training optimizer like stochastic gradient descent (SGD). We refer to this as the *high-entropy advantage* in this paper. To better understand the condition of this advantage, we further studied its correlation with the network width. Our results indicate that wider NNs tend to have a smaller high-entropy advantage for the same task (e.g. reaching the limit of generalization), which agrees with derivations under the infinite network width limit and the reported observations.<sup>26</sup>

## Results

### Arithmetic Question

We begun our investigation from small fully-connected neural networks (FNNs) on a relatively simple arithmetic task: learning a predefined equation of binary classification. Here we constructed a synthetic ‘spiral’ dataset, where every data point is a point on 2-D space with a color (brown or green) determined by its coordinates. More details including the equation used and figure of the generated dataset are presented in the Supplementary Materials. We generated 20 green points and 20 brown points randomly, forming two spirals. Our task is to predict whether a point is brown or green given its coordination. Therefore, this is a binary classification problem with 2 input features (horizontal and vertical coordinates).

We used Wang-Landau Monte Carlo (WLMC) method to sample the entropy landscape,  $S(L_{train}, A_{test})$ , as a function of the log-scaled train loss,  $\ln(L_{train})$ , and test accuracy,  $A_{test}$ . The log-scaled train loss allows us to better sample the low  $L_{train}$  states where the model converges after learning. In Fig. 1 (a), we presented the entropy landscape for a 4 layers  $\times$  8 neurons FNN (249 trainable parameters). Color gradient represents the entropy gradient, where warm color represents high entropy state. The WLMC method (and the Wang-Landau Molecular Dynamics method we will employ later) calculates the entropy with an algorithm-dependent zero point; thus, the absolute value of the entropy is meaningless, but the entropy difference between any two points in Fig. 1 (a) is meaningful. For each given  $\ln(L_{train})$ , we can calculate the corresponding equilibrium test accuracy using Equation 1:

$$\langle A_{test}(L_{train}) \rangle = \frac{\int_0^1 a \exp[S(L_{train}, a)] da}{\int_0^1 \exp[S(L_{train}, a)] da}. \quad (1)$$

where  $S$  is the entropy and  $a$  is variable standing for the test accuracy.  $\langle A_{test}(L_{train}) \rangle$  are plotted as magenta dots in Figure 1 (a) and we refer it as the *equilibrium accuracy* in this paper.

We then performed the classical training via the SGD optimizer for 100 times and collected the  $L_{train}$  versus  $A_{test}$  trajectories. For each given  $L_{train}$ , we calculated the mean  $A_{test}$ , which is plotted as the black curve in Figure 1 (a). For simplicity, we refer it as the *SGD accuracy* in this paper. We can see that when  $L_{train}$  reaches a low level ( $\ln L_{train} \approx -0.5$ ), the equilibrium accuracy increases rapidly with the decrease of  $L_{train}$  and gets saturated when  $\ln L_{train} \approx -3$ . In this regime, we observed a supremacy of the equilibrium accuracy over the SGD accuracy for each given  $\ln L_{train}$ , which indicates the existence of high-entropy advantage. Another interesting thing we noticed here is that when the training loss is at a high level ( $\ln L_{train} > 0$ ), the equilibrium accuracy is around 50%. This also agrees with our intuition, because when FNN has a high  $L_{train}$ , it generally suggests that the model does not learn anything yet but just making random guess, which should has an accuracy 50% for the binary classification.

We followed the same protocol and further tested on 3 additional FNN sizes and 2 different training time (see more details in Supplementary Materials). Results are presented in Figure 1 (b). Each point represents one training condition, and the black dashed line represents the level where equilibrium accuracy equals the SGD accuracy. Here we used the best SGD accuracy observed (i.e. the best-possible early stopping) and then looked for its corresponding equilibrium accuracy at the same train loss level. For all the 8 experiments conducted, the equilibrium accuracy outperforms the SGD accuracy with a large margin, further verifying that the high-entropy state can provide better generalization. The smallest FNN tested here (3 layers  $\times$  6 neurons) has 109 trainable parameters, which is still much larger than the number of training data points, 40, guaranteeing the overparameterized nature of all models.

### Kaggle House Price Prediction

After showing that high-entropy state can consistently provide better generalization for small FNNs, we then further extend the experiments to larger neural networks on real world tasks. Due to the increase of parameters number in large networks, WLMC

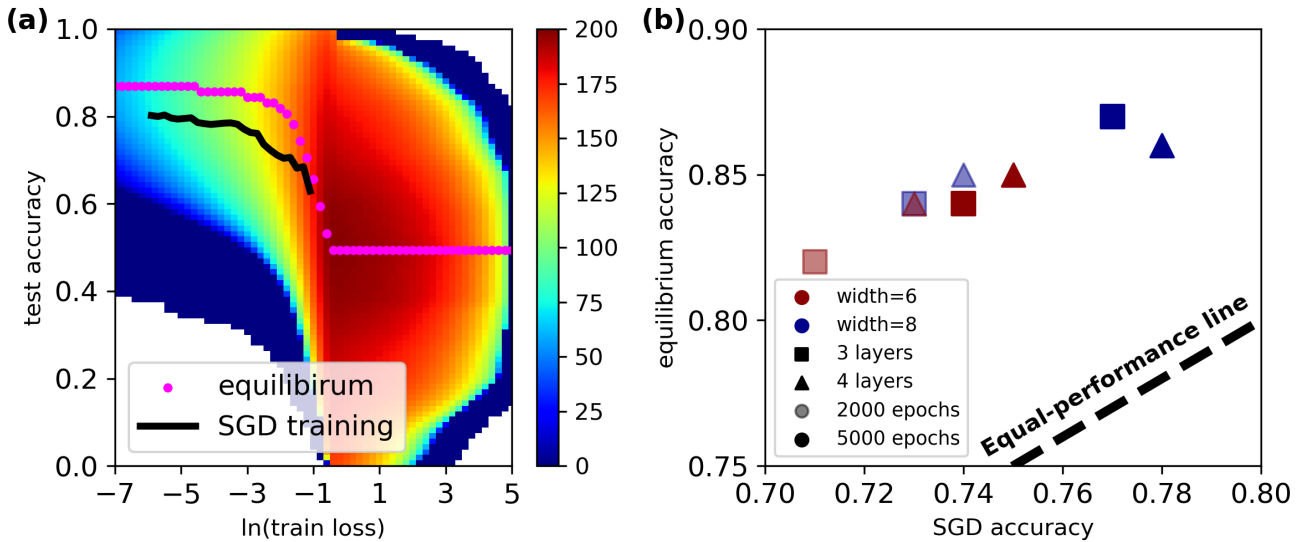


**Figure 1.** Entropy analysis via WLMC for arithmetic question: (a) Entropy landscape as a function of  $\ln(\text{train loss})$  and test accuracy. Color gradient represents the entropy gradient. (b) Equilibrium test accuracy versus the corresponding SGD test accuracy for 8 different NNs.

becomes inefficient, as it has a time complexity of  $\mathcal{O}(n)$  to update one parameter, where  $n$  is the total number of NNs’ trainable parameters. Therefore, we employed the Wang-Landau Molecular Dynamics (WLMC) method, which updates all  $n$  parameters together in each time step with time complexity  $\mathcal{O}(n)$ . (See Methods for more details)

We started from the House Price dataset<sup>27</sup> on Kaggle website<sup>28</sup>, where the task is to predict the house price from its descriptors like number of bedrooms and house age. For the sake of computational cost, here we only used the original training dataset which consists of 1460 houses. Each house has 79 descriptors (excluding the house ID) and we performed one-hot encoding for all categorical descriptors, yielding a total of 331 descriptors / features for each data point eventually. We randomly select 50% data as the train set, with the remaining data reserved for test. A 2-layer FNN is used for this regression task, where the hidden layer has 20 neurons. Therefore, the final model has 6661 trainable parameters, making it overparameterized.

Following the similar protocol described above for the arithmetic question, we got the entropy landscape,  $S(L_{\text{train}}, L_{\text{test}})$ , as a function of train loss,  $L_{\text{train}}$ , and test loss,  $L_{\text{test}}$ . Results are presented in Figure 2 (a), where both  $L_{\text{train}}$  and  $L_{\text{test}}$  are in log scale for better sampling the low loss regime. As in statistical physics, the probability distribution over different states (different locations in the plot) is sharply peaked around the entropy maximum, making the max-entropy state the thermodynamic equilibrium. We find out these max-entropy states at each  $L_{\text{train}}$ . We then performed the classical training via the SGD optimizer for 100 times and 3 different batch sizes, to make sure we have enough data points at each  $L_{\text{train}}$  value.  $L_{\text{train}} - L_{\text{test}}$  trajectories are collected and the mean  $\ln L_{\text{test}}$  at each  $\ln L_{\text{train}}$  are plotted as the black curve. The error bar for SGD training is smaller than the width of the black curve. Our results suggest that at a given  $L_{\text{train}}$ , the corresponding max entropy loss is significant lower than the test loss obtained via SGD training, suggesting the high-entropy advantage in NNs generalizability. More technical details, including data and hyperparameters tuning, are presented in Supplementary Materials.

### **MNIST Image: Handwritten Digit Recognition**

The modern neural networks have demonstrated remarkable success in the realm of computer vision<sup>29</sup>. One of the fundamental datasets used in the computer vision benchmark is the MNIST dataset, which consists of images with handwritten digits.<sup>30</sup> Here we used it to further verify that the high-entropy advantage for the computer vision task. Considering many models have presented 100% accuracy on the test set of MNIST (see Leaderboard of Kaggle Digit Recognizer competition<sup>31</sup>), we strategically increase the difficulty of the MNIST task by drastically reducing the size of training dataset. This is done by randomly sampling 500 images from the original dataset and dividing them equally as the train and test sets, respectively. We refer this dataset as the selected MNIST dataset in this paper and more details can be found in the Supplementary materials. The original MNIST dataset has 50,000 images for training, which is 200 times larger than ours. Thus, we expect this constraint can significantly intensify the task difficulties, so that we can better differentiate the potential advantage of the high-entropy states. We built a small convolutional neural network with 5 convolutional layers and one fully-connected layer. This network has 362 trainable parameters, which is larger than the training dataset (250 images) in the selected MNIST, making it an

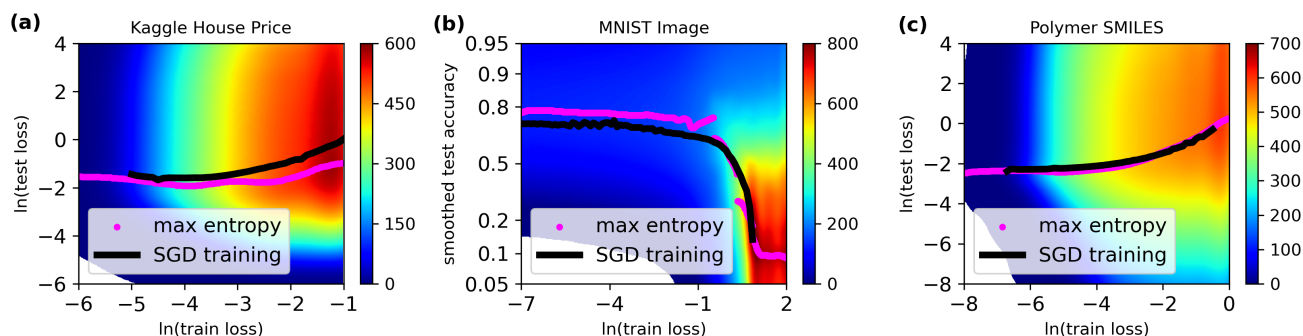


**Figure 2.** Entropy landscape of (a) Kaggle Housing Price dataset; (b) MNIST Image dataset; (c) Polymer SMILES dataset. For the SGD training of all three models, the standard error at each train loss level is smaller than the width of the curve.

overparamterized model.

In Figure 2 (b), we presented the entropy landscape,  $S(L_{train}, A_{test}^s)$ , of this neural network on the selected MNIST dataset. Here  $A_{test}^s$  is *smoothed accuracy* which is differentiable, as required by the WLMD algorithm (See Methods for details). We then find the max-entropy grid for each train loss on the landscape, which is again plotted as the magenta dots. Similar to the landscape in Figure 1 (a), we observed an increase of max entropy test accuracy when the train loss reaches a low level ( $L_{train} \approx -1$ ) and it gets saturated when  $\ln L_{train} \approx -4$ . When the train loss is high, we observed a high-entropy band around the test accuracy of 0.1. This also meets our expectation because the digit recognition is a 10-class classification problem, so random guesses should have an accuracy of 10%. We then performed the classical training via the SGD optimizer for 200 times. (See more details in Supplementary Materials) The mean SGD accuracy are plotted as the black curve. Our results suggest that for a given train loss, the corresponding max entropy accuracy generally outperforms the SGD training, especially when the train loss is small ( $\ln L_{train} < -2$ ).

In the Supplementary Materials, we further show the existence of the entropy advantage in a deeper neural network (10-layer ResNet<sup>29</sup>) on a selected CIFAR-10 dataset with 5,000 images.

### Polymer SMILES: Language Modeling

Natural language modeling is another domain where the neural networks have consistently outperformed traditional machine learning methods.<sup>2</sup> Language modeling is also inherently differs from other machine learning tasks due to its reliance on semantic complexity and contextuality.<sup>32</sup> Therefore, we further extended our tests to a language modeling dataset. We utilized the TransPolymer model published recently, which achieves state-of-the-art performance in all ten different downstream tasks for polymer property prediction.<sup>33</sup> TransPolymer is a BERT (Bidirectional Encoder Representations from Transformers) family model<sup>3,34</sup> and is pretrained on roughly 5 millions polymer SMILES augmented from the P11M database<sup>35</sup>. This pretrained transformer-based language model is able to take the SMILES as input directly and generate a 768-dimension embedding for each given SMILES. The embedding is then fed into a regressor head, a fully-connected layer with SiLU activation function, and is regressed on different polymer properties. Here we choose the Egb Dataset<sup>33,36</sup> to perform the entropy advantage experiment, which is the bandgap energy of bulk polymer and consists of 561 data points. This is the dataset where TransPolymer has the best performance (test  $R^2 = 0.93$ ), therefore, we can verify whether entropy advantage still exists for such a well-learned task. 80% data is used for training and the remaining 20% data is reserved for testing, which is same as the way reported in the original TransPolymer paper<sup>33</sup>.

For sampling efficiency, we follow the fintuning strategy of large foundation model<sup>33,37,38</sup>, where the encoder embedding is fixed and only tuning the regressor head of the TransPolymer model. We also reduced the width of the regressor to 50 while keep the SiLU activation function. Therefore, the final model has 38501 parameters, making it overparamterized. Entropy landscape of this language modeling task is presented in Figure 2 (c). As a regression problem, we found that the corresponding max-entropy loss at each  $L_{train}$  is slightly lower or comparable to its SGD training analog, which suggests that high-entropy state can generalize well. In other words, even for a task that could be well-learned via the SGD training, there is still a high-entropy advantage.

### Effect of Network Width

Now we have demonstrated high-entropy advantage in four distinct machine learning tasks, we will now study how is this advantage affected by the size of the neural network. It has been known that neural networks are equivalent to Gaussian processes in the limit of infinite width.<sup>39,40</sup> Previous experiments also indicated that the performance of optimized neural

networks converges to the corresponding Gaussian Process with increasing network width.<sup>40</sup> Consequently, it is reasonable to expect the high-entropy advantage could also change as a function of the network width.

To better evaluate this, we constructed a Spiral Regression Dataset (see Supplementary Materials for details) which consists of 500 data points and is divided equally for train and test sets. Using the same WLMD method, we constructed the entropy landscapes on NNs with four different widths,  $W$ , ranging from 30 to 1000. All four models are overparameterized and the largest one has more than 1 million trainable parameters. Figure 3 presents the entropy landscapes of different networks and our results suggest that narrower networks possess more significant entropy advantage, which finally fades away when  $W = 1000$ . Note here we used the Adam optimizer because the SGD optimizer performs much poorer. We also performed the same experiments on the Kaggle House price prediction, the selected MNIST image recognition, and the Polymer SMILES language modeling tasks and observed the similar trend: entropy advantage is more significant for narrower networks (See Figure 7 - 9 in the Supplementary Materials).

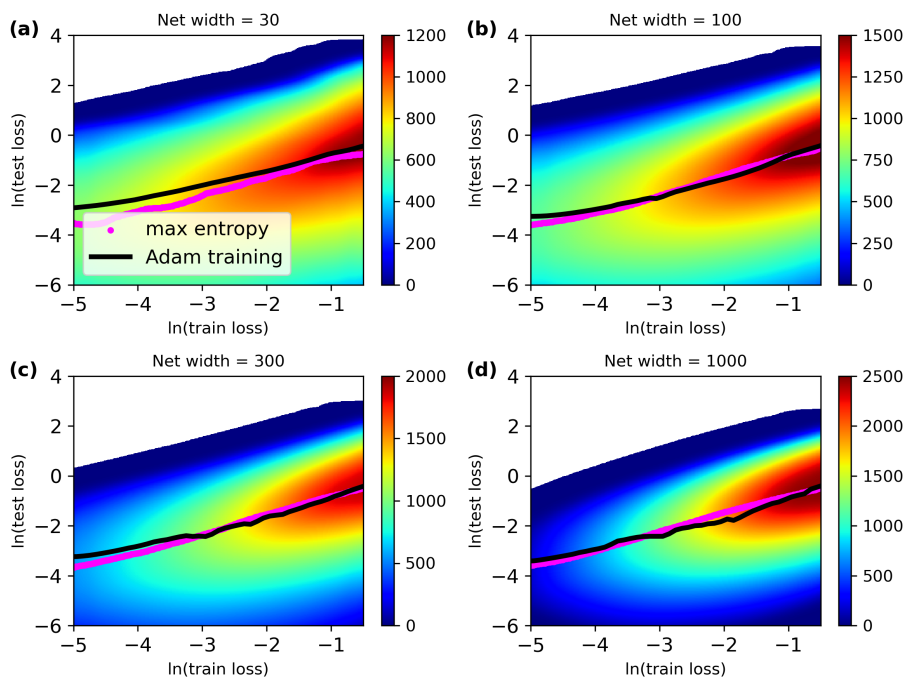


**Figure 3.** Entropy landscape on spiral regression task with different NN width: (a) 30; (b) 100; (c) 300; (d) 1000.

## Discussion

In this paper, we investigated the relationship between the entropy and generalizability of neural networks (NNs). We performed experiments in four distinctive machine learning tasks, covering arithmetic questions, real world tabular data, computer vision, and language modeling. WLMC and WLMD methods are used to sample the NNs' entropy landscapes for both classification ( $S(L_{train}, A_{test})$ ) and regression tasks ( $S(L_{train}, L_{test})$ ). For classification tasks, a smoothed test accuracy is employed for WLMD-simulated networks to guarantee the differentiability. At high train loss ( $L_{train}$ ), the max-entropy states achieve random-guess accuracies, supporting the validity of the Wand-Landau-based algorithm in sampling the entropy of NNs. For networks with low train loss value, the max-entropy states generally achieve higher accuracy than the SGD-trained states. For regression tasks, the max-entropy states have lower or at least comparable test loss at all levels of train loss.

Our contributions are two-fold. First, such a high-entropy advantage may be widely present in different neural networks architectures and learning tasks. If so, our work shed lights on a new approach to enhancing model performance without changing its architecture: developing optimizers that can effectively find NNs' equilibrium (max entropy) states. This could be achieved by methods like low-temperature Newtonian molecular dynamics simulations or simulated annealing. Second, the high-entropy advantage also hints on a potential theoretical explanation for the generalizability of overparametrized models after SGD training. The SGD training algorithm minimizes the loss function using an estimated the gradient of the loss function. The inaccuracy involved in such estimation may bias the trained NN toward higher-entropy minima, which possess higher generalizability.

While there are many studies focusing on using machine learning models to solve problems in physics<sup>41-45</sup>, the reverse



directions retains much less attention. However, the foundation concepts of machine learning, especially for neural networks, are deeply rooted in physics. This historic connection is exemplified by the pioneering work including the Hopfield networks<sup>46,47</sup> and the Boltzmann machine<sup>48,49</sup>, which is draw directly from principles of statistical mechanics. We believe our work (re)highlights the potential of treating NNs as physical systems, promoting possibilities to apply well-established statistical physics methods to aid machine learning research. It would be intriguing to explore how techniques like simulated annealing or parallel tempering could accelerate the searching process of NNs' equilibrium state. While a few studies have explored this direction before<sup>50,51</sup>, the existence of the high-entropy advantage in NNs underscores the great potential of further research.

## Methods

### Wand-Landau Monte Carlo for Neural Networks

WLMC is employed for the Spiral Classification Dataset and our results are averaged over 6 independently generated training and testing datasets. For each dataset, 10,000 stages simulations has been performed, where each stage contains  $3.2 \times 10^6$  steps. In each step, we randomly change one parameter in the network and then evaluate both train loss and test accuracy. Therefore, WLMC algorithm has a time complexity of  $O(N)$  to update one trainable parameter, where  $N$  is the total number of parameters in the network. We also employed an adapted step size during the simulation by calculating the accepting rate for every 1000 steps. The step size is increased by 10% if the rate is higher than 0.7 and is decreased by 10% when it is lower than 0.3. The 'modification factor' in original Wang-Landau method<sup>52</sup> is set to be  $f = \exp[5/(n + 10)]$  for the  $n$ th stage.

Parameters in the neural networks ranges from  $-\infty$  to  $\infty$ , when no constraint is added. Therefore, the volume of a parameter space is infinite, even for a tiny neural network. On the other hand, to make the thermodynamic quantities valid we must prescribe finite ranges for the parameters. According to early-established experience in neural network training, to alleviate the exploding-gradient and diminishing-gradient problems, the weight parameters should be on the order of  $1/\sqrt{W}$ <sup>53</sup>. Thus, we limit weight parameters to the range of  $[-2/\sqrt{W}, 2/\sqrt{W}]$  for our WLMC simulation.

### Wand-Landau Molecular Dynamics for Neural Networks

When sampling the entropy landscape of practical neural networks with tens of thousands parameters, WLMC becomes too expensive as it needs to perform the entire forward propagation to update one parameter. Therefore, we employed the WLMD method proposed before<sup>54,55</sup>, which has a time complexity of  $O(N)$  to update  $N$  parameters, where  $N$  is the total number of trainable parameters in the network. In addition, a Langevin thermostat is implemented to achieve the smooth temperature control during the simulation. The weight parameters are constrained by the range of  $[-2/\sqrt{W}, 2/\sqrt{W}]$  and a reflecting boundary is applied. We also find that the range of the weights does not qualitatively change our results within a reasonable range.

Unlike WLMC, the WLMD algorithm can only directly calculate the entropy as a function of differentiable variables. In order to calculate  $S$  as a function of  $A_{test}$ , we designed a "smoothed" approximation of the test accuracy:

$$A_{test}^s = S(\alpha \times \delta l), \quad (2)$$

where  $S(x) = 1/[1 + \exp(-x)]$  is the sigmoid function,  $\alpha$  is a hyperparameter, and  $\delta l$  is the difference between the logit of the correct answer and the highest logit of incorrect answers. In the  $\alpha \rightarrow \infty$  limit, we would have  $A_{test}^s = A_{test}$ . When  $\alpha$  is finite,  $A_{test}^s$  becomes a differentiable approximation of  $A_{test}$ . In practice we choose  $\alpha = 5$ . This leads to a smoothing error,  $|A_{test}^s - A_{test}|$ , that is always smaller than 1.5% except for the initial  $10^7$  MD time steps. The initial part of the simulation have significantly higher smoothing errors (as much as 30%), but that does not affect the correctness of our final results since WLMD has the capability of starting from an incorrect entropy landscape and gradually converging to the correct entropy landscape.

The starting entropy  $S(x, y)$ , where  $x = \ln(L_{train})$  and  $y = \ln(L_{test})$  or  $y = A_{test}^s$ , is not zero but rather

$$S_{init}(x, y) = c_i(x - x_{max})^2 H(x - x_{max}) + c_i(y - y_{max})^2 H(y - y_{max}), \quad (3)$$

where  $c_i = 3000$  is a constant and  $H(x) = \begin{cases} 0, & x < 0 \\ 1, & x \geq 0 \end{cases}$  is the Heaviside step function. Parameters  $x_{max}$  and  $y_{max}$  are system-dependent and listed in the supplementary material. By starting with such an  $S_{init}$ , we make the algorithm concentrate its exploration effort in the  $x < x_{max}$  and  $y < y_{max}$  regime, improving efficiency.

For stable simulation, the scale factor in our simulation follows the schedule

$$f(t) = \begin{cases} \frac{t}{t_1} f_{max} & t \leq t_1 \\ f_{max} & t_1 < t \leq t_2 \\ \frac{t_2 - t_3}{t - t_3} f_{max} & t > t_2 \end{cases}, \quad (4)$$

where  $f_{\max}$ ,  $t_1$ ,  $t_2$ , and  $t_3$  are parameters of the schedule. For each step, instead of adding one count to the corresponding position on the entropy landscape, a small Gaussian distribution is added to smooth the sampled entropy landscape. Numerical details of all parameters employed for different machine learning tasks can be found in the Supplementary materials.

## References

1. Deng, J. *et al.* Imagenet: A large-scale hierarchical image database. In *2009 IEEE conference on computer vision and pattern recognition*, 248–255 (Ieee, 2009).
2. Vaswani, A. *et al.* Attention is all you need. *Adv. neural information processing systems* **30** (2017).
3. Devlin, J., Chang, M.-W., Lee, K. & Toutanova, K. Bert: Pre-training of deep bidirectional transformers for language understanding. *arXiv preprint arXiv:1810.04805* (2018).
4. Brown, T. *et al.* Language models are few-shot learners. *Adv. neural information processing systems* **33**, 1877–1901 (2020).
5. Srivastava, N., Hinton, G., Krizhevsky, A., Sutskever, I. & Salakhutdinov, R. Dropout: a simple way to prevent neural networks from overfitting. *The journal machine learning research* **15**, 1929–1958 (2014).
6. Zhang, C., Bengio, S., Hardt, M., Recht, B. & Vinyals, O. Understanding deep learning requires rethinking generalization. *Commun. ACM* **64**, DOI: [10.1145/3446776](https://doi.org/10.1145/3446776) (2016).
7. Ying, X. An overview of overfitting and its solutions. In *Journal of physics: Conference series*, vol. 1168, 022022 (IOP Publishing, 2019).
8. Zhang, C., Bengio, S., Hardt, M., Recht, B. & Vinyals, O. Understanding deep learning (still) requires rethinking generalization. *Commun. ACM* **64**, 107–115 (2021).
9. Neyshabur, B., Bhojanapalli, S., McAllester, D. & Srebro, N. Exploring generalization in deep learning. *Adv. neural information processing systems* **30** (2017).
10. Allen-Zhu, Z., Li, Y. & Liang, Y. Learning and generalization in overparameterized neural networks, going beyond two layers. *Adv. neural information processing systems* **32** (2019).
11. Zou, D. & Gu, Q. An improved analysis of training over-parameterized deep neural networks. *Adv. neural information processing systems* **32** (2019).
12. Silver, D. *et al.* Mastering the game of go without human knowledge. *nature* **550**, 354–359 (2017).
13. Jumper, J. *et al.* Highly accurate protein structure prediction with alphafold. *Nature* **596**, 583–589 (2021).
14. Merchant, A. *et al.* Scaling deep learning for materials discovery. *Nature* **624**, 80–85 (2023).
15. Keskar, N. S., Mudigere, D., Nocedal, J., Smelyanskiy, M. & Tang, P. T. P. On large-batch training for deep learning: Generalization gap and sharp minima. *arXiv preprint arXiv:1609.04836* (2016).
16. Jiang, Y., Neyshabur, B., Mobahi, H., Krishnan, D. & Bengio, S. Fantastic generalization measures and where to find them. *arXiv preprint arXiv:1912.02178* (2019).
17. Fort, S. & Scherlis, A. The goldilocks zone: towards better understanding of neural network loss landscapes. In *Proceedings of the Thirty-Third AAAI Conference on Artificial Intelligence and Thirty-First Innovative Applications of Artificial Intelligence Conference and Ninth AAAI Symposium on Educational Advances in Artificial Intelligence*, 3574–3581 (2019).
18. Ansuini, A., Laio, A., Macke, J. H. & Zoccolan, D. Intrinsic dimension of data representations in deep neural networks. *Adv. Neural Inf. Process. Syst.* **32** (2019).
19. Dinh, L., Pascanu, R., Bengio, S. & Bengio, Y. Sharp minima can generalize for deep nets. In *International Conference on Machine Learning*, 1019–1028 (PMLR, 2017).
20. Feng, Y., Zhang, W. & Tu, Y. Activity–weight duality in feed-forward neural networks reveals two co-determinants for generalization. *Nat. Mach. Intell.* **5**, 908–918 (2023).
21. Neyshabur, B., Tomioka, R. & Srebro, N. In search of the real inductive bias: On the role of implicit regularization in deep learning. *arXiv preprint arXiv:1412.6614* (2014).
22. Neyshabur, B. Implicit regularization in deep learning. *arXiv preprint arXiv:1709.01953* (2017).
23. Keskar, N. S. & Socher, R. Improving generalization performance by switching from adam to sgd. *arXiv preprint arXiv:1712.07628* (2017).

24. Zhou, P. *et al.* Towards theoretically understanding why sgd generalizes better than adam in deep learning. *Adv. Neural Inf. Process. Syst.* **33**, 21285–21296 (2020).
25. Gupta, A., Ramanath, R., Shi, J. & Keerthi, S. S. Adam vs. sgd: Closing the generalization gap on image classification. In *OPT2021: 13th Annual Workshop on Optimization for Machine Learning*, 1–7 (2021).
26. Lee, J. *et al.* Deep neural networks as gaussian processes. *arXiv preprint arXiv:1711.00165* (2017).
27. De Cock, D. Ames, iowa: Alternative to the boston housing data as an end of semester regression project. *J. Stat. Educ.* **19** (2011).
28. Montoya, A. & DataCanary. House prices - advanced regression techniques. <https://kaggle.com/competitions/house-prices-advanced-regression-techniques> (2016). Kaggle.
29. He, K., Zhang, X., Ren, S. & Sun, J. Deep residual learning for image recognition. In *Proceedings of the IEEE conference on computer vision and pattern recognition*, 770–778 (2016).
30. Deng, L. The mnist database of handwritten digit images for machine learning research [best of the web]. *IEEE signal processing magazine* **29**, 141–142 (2012).
31. AstroDave & Cukierski, W. Digit recognizer. <https://kaggle.com/competitions/digit-recognizer> (2012). Kaggle.
32. Liu, N. F., Gardner, M., Belinkov, Y., Peters, M. E. & Smith, N. A. Linguistic knowledge and transferability of contextual representations. *arXiv preprint arXiv:1903.08855* (2019).
33. Xu, C., Wang, Y. & Barati Farimani, A. Transpolymer: a transformer-based language model for polymer property predictions. *npj Comput. Mater.* **9**, 64 (2023).
34. Liu, Y. Roberta: A robustly optimized bert pretraining approach. *arXiv preprint arXiv:1907.11692* **364** (2019).
35. Ma, R. & Luo, T. Pi1m: a benchmark database for polymer informatics. *J. Chem. Inf. Model.* **60**, 4684–4690 (2020).
36. Kuenneth, C. *et al.* Polymer informatics with multi-task learning. *Patterns* **2** (2021).
37. Chithrananda, S., Grand, G. & Ramsundar, B. Chemberta: large-scale self-supervised pretraining for molecular property prediction. *arXiv preprint arXiv:2010.09885* (2020).
38. Ahmad, W., Simon, E., Chithrananda, S., Grand, G. & Ramsundar, B. Chemberta-2: Towards chemical foundation models. *arXiv preprint arXiv:2209.01712* (2022).
39. Neal, R. M. & Neal, R. M. Priors for infinite networks. *Bayesian learning for neural networks* 29–53 (1996).
40. Lee, J. *et al.* Deep neural networks as gaussian processes. In *International Conference on Learning Representations* (2018).
41. Raissi, M., Perdikaris, P. & Karniadakis, G. E. Physics-informed neural networks: A deep learning framework for solving forward and inverse problems involving nonlinear partial differential equations. *J. Comput. physics* **378**, 686–707 (2019).
42. Udrescu, S.-M. & Tegmark, M. Ai feynman: A physics-inspired method for symbolic regression. *Sci. Adv.* **6**, eaay2631 (2020).
43. Yang, E. & Riggleman, R. A. Role of local structure in the enhanced dynamics of deformed glasses. *Phys. Rev. Lett.* **128**, 097801 (2022).
44. Wang, H. *et al.* Scientific discovery in the age of artificial intelligence. *Nature* **620**, 47–60 (2023).
45. Xiao, H. *et al.* Identifying microscopic factors that influence ductility in disordered solids. *Proc. Natl. Acad. Sci.* **120**, e2307552120 (2023).
46. Hopfield, J. J. Neural networks and physical systems with emergent collective computational abilities. *Proc. national academy sciences* **79**, 2554–2558 (1982).
47. Hopfield, J. J. Neurons with graded response have collective computational properties like those of two-state neurons. *Proc. national academy sciences* **81**, 3088–3092 (1984).
48. Ackley, D. H., Hinton, G. E. & Sejnowski, T. J. A learning algorithm for boltzmann machines. *Cogn. science* **9**, 147–169 (1985).
49. Hinton, G. E., Sejnowski, T. J. *et al.* Learning and relearning in boltzmann machines. *Parallel distributed processing: Explor. microstructure cognition* **1**, 2 (1986).
50. Zheng, G., Sang, J. & Xu, C. Understanding deep learning generalization by maximum entropy. *arXiv preprint arXiv:1711.07758* (2017).



51. Gabrié, M. *et al.* Entropy and mutual information in models of deep neural networks. *Adv. neural information processing systems* **31** (2018).
52. Wang, F. & Landau, D. P. Efficient, multiple-range random walk algorithm to calculate the density of states. *Phys. review letters* **86**, 2050 (2001).
53. Glorot, X. & Bengio, Y. Understanding the difficulty of training deep feedforward neural networks. In *Proceedings of the thirteenth international conference on artificial intelligence and statistics*, 249–256 (JMLR Workshop and Conference Proceedings, 2010).
54. Kim, J., Straub, J. E. & Keyes, T. Statistical-temperature monte carlo and molecular dynamics algorithms. *Phys. review letters* **97**, 050601 (2006).
55. Junghans, C., Perez, D. & Vogel, T. Molecular dynamics in the multicanonical ensemble: Equivalence of wang–landau sampling, statistical temperature molecular dynamics, and metadynamics. *J. chemical theory computation* **10**, 1843–1847 (2014).
56. Patra, A. *et al.* A multi-fidelity information-fusion approach to machine learn and predict polymer bandgap. *Comput. Mater. Sci.* **172**, 109286 (2020).

## Acknowledgements

The authors thank National Natural Science Foundation of China for supporting this research (Grant 12405043). We also thank computational resources provided by Bridges-2 at Pittsburgh Supercomputing Center through ACCESS allocation CIS230096.

## Author contributions

E. Y. and G. Z. conceived the research, performed simulations, and analyzed data. All authors participated in discussions, writing, and proofreading of the manuscript.

## Competing interests

The authors declare no competing interests.

## Supplementary Materials

### Newtonian MD results for MNIST dataset

To verify the correctness of the entropy diagram calculated from Wang-Landau MD simulations, we performed regular (Newtonian) MD of the MNIST system. We observed that as the system evolves and approaches equilibrium, the test accuracy indeed increases and approaches the high-entropy value.

The MD simulation was performed at temperature  $k_B T = 0.005$  with Langevin thermostat, and the system eventually equilibrates at potential energy  $E_p = L_{\text{train}} \approx 0.04$ . From the entropy diagram (Fig. 2b), at this  $L_{\text{train}}$  the equilibrium test accuracy is around 0.76, while SGD training achieved a test accuracy of 0.68. Our MD results are presented in Fig. 4. The test accuracy is indeed slowly increasing and approaching 0.76, but the train loss is also slowly decreasing. Since the test accuracy can increase due to either decreasing train loss or increasing entropy (as time increases), we further performed a separation-of-variables study by plotting the test accuracy for only the time steps with the train loss within a small window of  $0.04 < L_{\text{train}} < 0.041$ . For this case, the test accuracy still increases over time, which is a strong evidence that the test accuracy is indeed positively correlated with entropy.

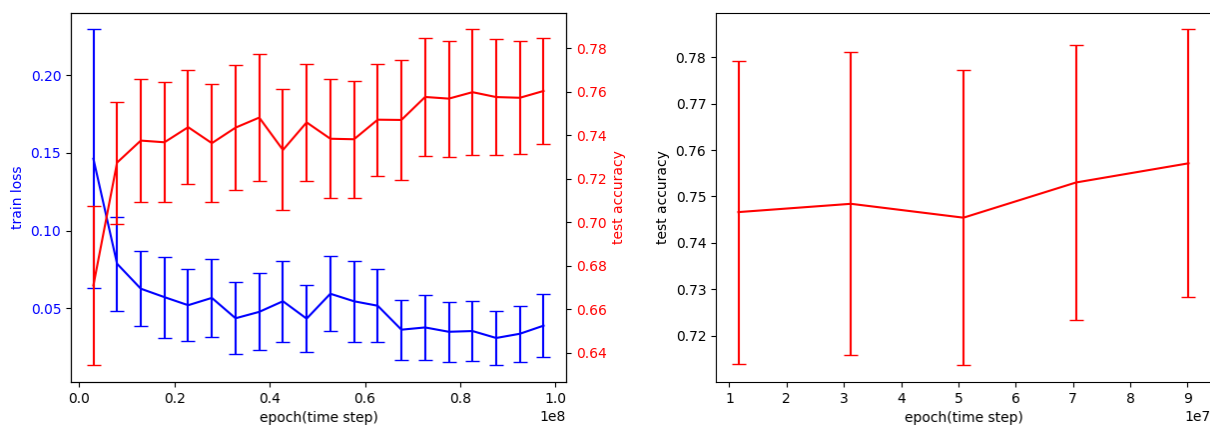


**Figure 4.** (left) The train loss (energy) and test accuracy versus time steps (epoches) during Newtonian molecular dynamics simulations of the MNIST system. We averaged over 4 independent instances of simulations to reduce noise. (right) The test accuracy at time steps for which the train loss is in a small range of  $0.04 < L_{\text{train}} < 0.041$ . Note that the length of error bars indicate the standard deviations of individual instances of neural networks, not the error estimation of each data point.

## Dataset Details

### Spiral Dataset

We generated the spiral dataset using the following equations:

$$\begin{aligned}(x_{1i}, x_{2i}) &= (r_i \cos \theta_i + N_{1i}, r_i \sin \theta_i + N_{2i}) \\ \theta_i &= 2r_i + \pi y_i\end{aligned}\tag{5}$$

where  $x_{1i}$  and  $x_{2i}$  are the horizontal and vertical coordinates of a point,  $r_i$  is uniformly distributed between 1 and 5, and  $y_i$  is the label (*i.e.*, color) of a point. Both  $N_{1i}$  and  $N_{2i}$  are Gaussian random noises with mean 0 and standard deviation 0.1.

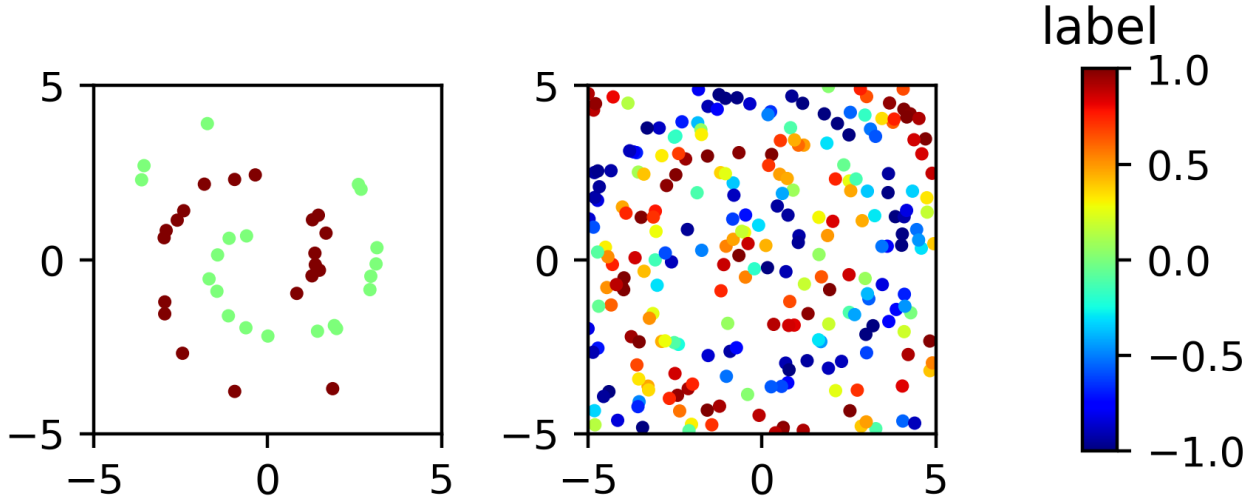


**Figure 5.** (left) The spiral dataset. An independent test set was then generated following exactly the same procedure but with a different random seed. (right) Same left, except for the spiral regression dataset with 250 points.

### Spiral Regression Dataset

We generated the spiral regression datasets by first generating random coordinates,  $-5 < x_{1i} < 5$  and  $-5 < x_{2i} < 5$ , for  $N = 50, 100,$  or  $250$  points. We then calculate the label (color) of each point using the formula

$$y_i = \sin(\theta_i - 2r_i),\tag{6}$$

where  $r_i$  and  $\theta_i$  are the polar coordinates of the  $i$ th point.

### Kaggle House Price Dataset

The Kaggle House Price dataset is collected from the Kaggle website.<sup>28</sup> Here we used the training data which consist of 1,460 house sale prices with 79 descriptors (like lot area and street type of the house). This tabular data is processed to better fit it into the neural network modeling. All the descriptors are divided into two groups: numerical features and categorical features. For numerical features, we performed standard scaling so that the data have a mean of 0 and a variance of 1. For categorical features, we performed one-hot encoding. After processing the raw data, we end up a new dataset which consists of 331 features. Therefore, our FNNs for the Kaggle House Price Prediction task have a input layer of 331 units. To make this learning task more difficult, we randomly selected 50% data as the train set and the remaining 50% data is used as the test set.

### Selected MNIST Dataset

The MNIST handwritten digits dataset is downloaded using the torchvision Python package. We randomly selected 250 images for the training dataset and 250 images for the test dataset. We greatly reduced size of the dataset in order to increase the difficulty of machine learning and decrease the simulation time.

### ***Polymer SMILES Dataset***

The Polymer SMILES dataset is collected from the TransPolymer work<sup>33</sup>, which is the foundation chemical language model we used in this study. The dataset is originally built by Ramprasad and coauthors, which consists of 561 polymer SMILES strings and their bulk electric band gap energy (eV)<sup>36,56</sup>. TransPolymer takes SMILES strings directly into the encoder, which is pretrained over 5 millions polymer SMILES string via mask language modeling<sup>33</sup>. This pretrained encoder can generate an embedding vector with a dimension of 768 for each polymer SMILES, which is then fed into the regressor head for downstream task learning. For sampling efficiency, we fixed the encoder of TransPolymer and only finetuning the regressor head, which is also commonly employed strategy for language model fine-tuning<sup>33,37,38</sup>. We follow the same protocol reported in the original TransPolymer work and randomly selected 80% data for train set and the remaining 20% data is used as test set.

## Neural network and training parameters

To benchmark the max-entropy state, we trained the corresponding neural networks for each task via the SGD optimizer. For a given network architecture, two hyperparameters have been tuned including learning rate and batch size. Best hyperparameters for different neural networks can be found in Table 1 to 5. Note for Kaggle House Price Prediction task, three different batch sizes have been employed for all neural networks to collect enough data for the full range of train loss. To make sure we are comparing max-entropy state with the best-available SGD training state, we always select the lowest test loss value for SGD training if there are more than one network falls into the bin of a certain train loss level. After determining the best training hyperparameters, we trained 100 neural networks and collected the train loss-test loss trajectories (regression task) or the train loss- test accuracy (classification task) during the entire training process of each task. These trajectories are then used to calculate the SGD training curves presented in Figure 1 to 3.

Network Width	Number of parameters	Best LR	Best Batch Size	LR Optimized Range	Batch Size Optimized Range
10	3331	5e-4	16	[1e-4, 1e-2]	[16, 128]
20	6661	5e-4	16	[1e-4, 1e-2]	[16, 128]
50	16651	5e-3	16	[1e-4, 1e-2]	[16, 128]
100	33200	8e-3	64	[1e-4, 1e-2]	[16, 128]

**Table 1.** Hyperparameters tuning details for Kaggle House Price Prediction

Network Width	Number of parameters	Best LR	Best Batch Size	LR Optimized Range	Batch Size Optimized Range
2 channels	362	0.003	4	[0.001, 0.1]	[4, 256]
3 channels	646	0.003	4	[0.001, 0.1]	[4, 256]
4 channels	1002	0.003	4	[0.001, 0.1]	[4, 256]

**Table 2.** Hyperparameters tuning details for MNIST Digit Recognition

Network Width	Number of parameters	Best LR	Best Batch Size	LR Optimized Range	Batch Size Optimized Range
2	1541	5e-3	32	[1e-4, 1e-1]	[16, 128]
10	7701	1e-2	32	[1e-4, 1e-1]	[16, 128]
50	38501	1e-2	64	[1e-4, 1e-1]	[16, 128]
100	77001	1e-2	64	[1e-4, 1e-1]	[16, 128]

**Table 3.** Hyperparameters tuning details for Language Modeling on Polymer SMILES

Network Width	Number of parameters	Best LR	Best Batch Size	LR Optimized Range	Batch Size Optimized Range
30	1051	2e-3	5	[5e-5, 2e-2]	[5, 25]
100	10501	5e-3	10	[5e-5, 2e-2]	[5, 25]
300	91501	2e-3	5	[5e-5, 2e-2]	[5, 25]
1000	1005001	2e-3	10	[5e-5, 2e-2]	[5, 25]

**Table 4.** Hyperparameters tuning details for spiral regression. For this dataset, we tuned the hyperparameters using the largest dataset ( $N = 250$ ) only since the smaller datasets yielded poorer results. We also switched to Adam optimizer since SGD yielded poor results.



Network Width	Number of parameters	Best LR	Best Batch Size	LR Optimized Range	Batch Size Optimized Range
6-12 channels	43604	1e-4	64	[1e-5, 2e-2]	[32, 256]

**Table 5.** Hyperparameters tuning details for CIFAR dataset. For this dataset, we did not experiment with different neural-network widths due to high computational cost.

### WLMD Simulation Parameters Summary

WLMD Parameters	Kaggle House	MNIST	Polymer SMILES	CIFAR	Spiral Regression
Gaussian Sigma	0.5	0.2	0.5	0.3	0.2
Gaussian Cutoff	2	0.8	2	1.2	0.8
Max ln(Train Loss)	-1.0	2.0	0.0	1.0	-0.5
Max ln(Test Loss) or smoothed Accuracy	5.0	0.95	5.0	1.0	$\infty$ (no constraint)
$f_{\max}$	20	3	20	20	5
$t_1$	5e5	2e5	1e6	3e5	2e5
$t_2$	5e5	1e7	1e6	2e6	1e7
$t_3$	0	8e6	0	0	8e6
Timestep	1e-4	3e-6	3e-5	2e-5	5e-5
Langevin Thermostat Friction Coefficient	0.01	1e-5	0.01	1e-4	3e-5

**Table 6.** WLMD Simulation Parameters for Different Machine Learning Tasks.

### Entropy Advantage for ResNet on selected CIFAR dataset

To confirm the existence of entropy advantage in deeper neural networks with more complex architectures, we have constructed a 10-layer ResNet<sup>29</sup>. The neural network consists of an initial convolutional layer with 6 channels, and then 4 residual blocks with 6, 12, 12, and 12 channels each, and a final fully-connected layer. The original ResNet architecture contains batch-normalization operations, which breaks the rigorous analogy between training losses and physical energy landscapes. Therefore, we replaced all of them with layer normalization operations. Our training and test datasets each contain 2500 randomly chosen images of either a deer or a frog from the CIFAR-10 dataset. Due to the significantly higher computational cost, we only ran WLMD for  $3 \times 10^7$  time steps for this system. Nevertheless, our result in Fig. 6 clearly shows an entropy advantage.

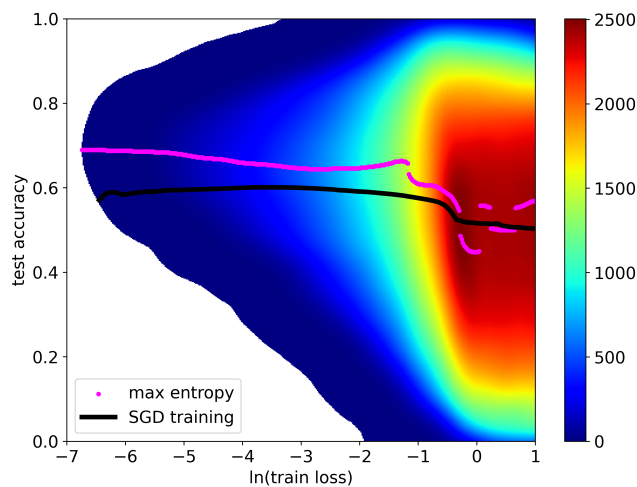


**Figure 6.** Entropy landscape of ResNet on the selected CIFAR dataset

### High Entropy Advantages Analysis

As presented in Figure 3, the high entropy advantage is more significant when the neural network is narrower, on the spiral regression task. To further validate this observation, we performed same tests on the other three tasks including Kaggle House Price prediction, MNIST digit recognition, and Polymer SMILES Language modeling. We found the similar trend in all three tasks: narrow networks present larger high-entropy advantage. Detailed results are presented in Figure 7 to 9.

#### Kaggle House Price Prediction

For Kaggle House Price prediction, we tested four different neural networks. Each network has 1 hidden layer, where the width,  $W$ , varies from 10 to 100. Our experiments suggest that the gap between the max-entropy curve and the SGD training curve becomes smaller (and almost disappeared at  $W = 100$ ) with the increase of  $W$ .

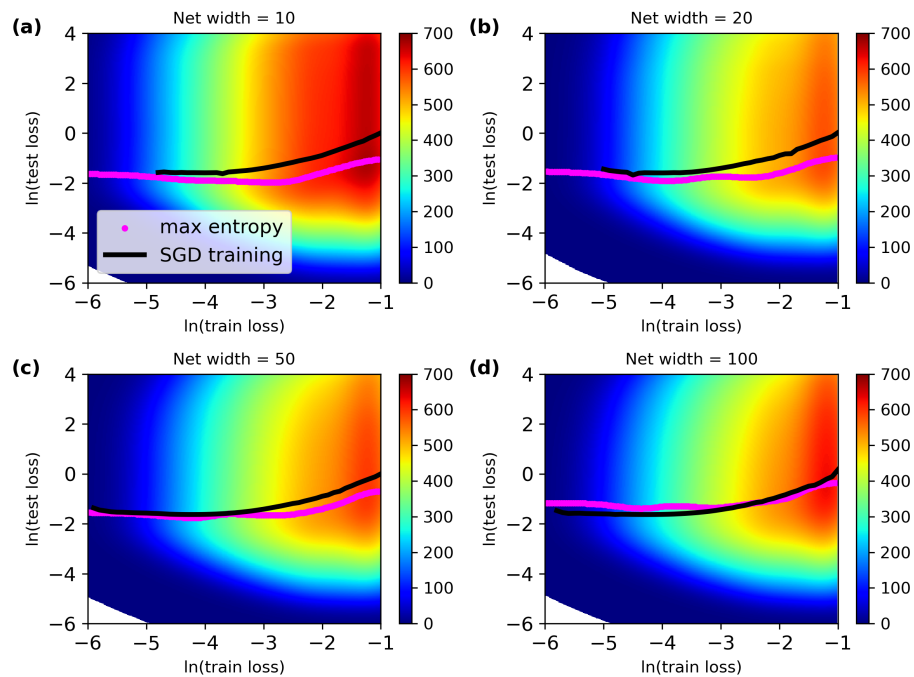


**Figure 7.** Entropy landscape of Kaggle House Price prediction task with different neural network width,  $W$ : (a)  $W = 10$ ; (b)  $W = 20$ ; (c)  $W = 50$ ; (d)  $W = 100$ .

### MNIST Digit Recognition

CNN is used in our experiment on the MNIST Digit Recognition task. Therefore, to evaluate the effect of network width on the high entropy advantage, we varied the channel number and tested three different CNNs. Results are presented in Figure 8. While CNNs with 3 and 4 channels present similar level of advantage, the max-entropy state of the 2-channel CNN has significantly higher test accuracy when train loss is small.

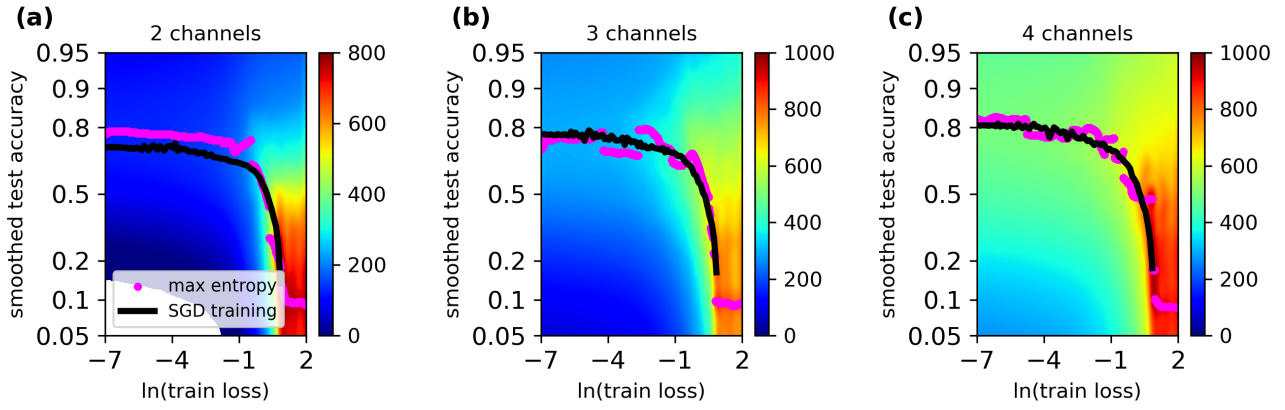


**Figure 8.** Entropy landscape of MNIST Digit Recognition task with different channel numbers: (a) 2; (b) 3; (c) 4.

### Polymer SMILES Language Modeling

We focused on the regressor head of the TransPolymer<sup>33</sup> model in Polymer SMILES language modeling task, which is a linear layer. Therefore, we varied its width from 2 to 100 to evaluate the high entropy advantage at different network width. As we mentioned in the main text, this is a well-learned task with test  $R^2 > 0.9$  for all four regressor heads we trained using SGD (see Figure 10). However, max-entropy state is still slightly better than the SGD training state when  $W = 10$  (Figure 9 (b)). For increased width  $W = 50$  and  $W = 100$ , the max-entropy state performs *equally well* with SGD training in at all training losses (Figure 9 (c) and (d)). When we use an extremely narrow network where  $W = 2$ , we can see a significant gap between the max-entropy curve and the SGD training curve. (Figure 9 (a)) While the entropy landscape of in Figure 9 looks different from the others, two independent experiments have been ran to make sure that it is not due to randomness. We speculate this distinct shape of entropy landscape is due to the extreme narrow regressor head employed ( $W = 2$ ).

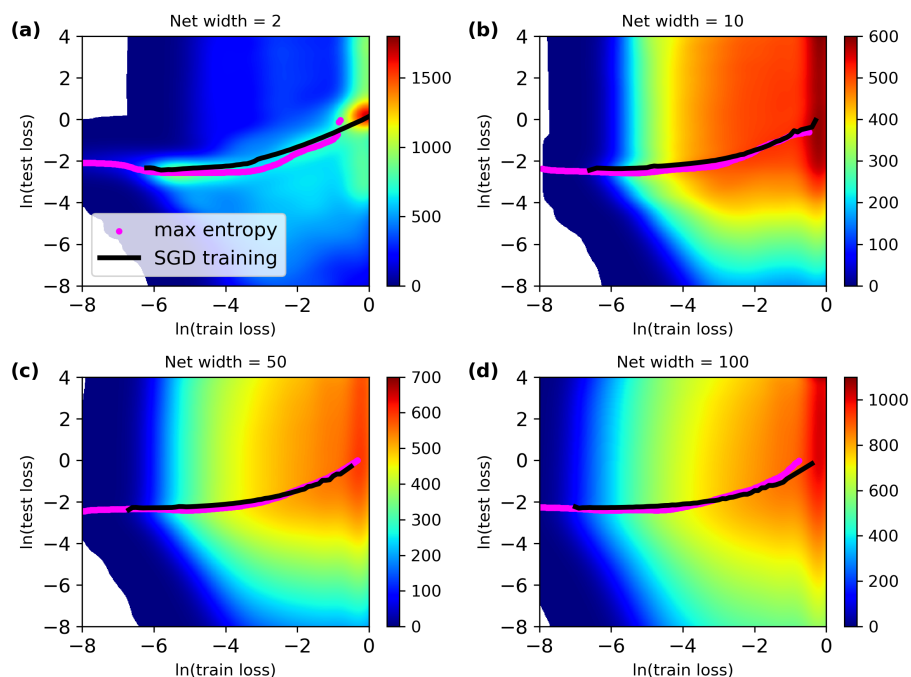


**Figure 9.** Entropy landscape of Polymer SMILES language modeling with different regressor head widths,  $W$ : (a)  $W=2$ ; (b)  $W=10$ ; (c)  $W=50$ ; (d)  $W=100$ .

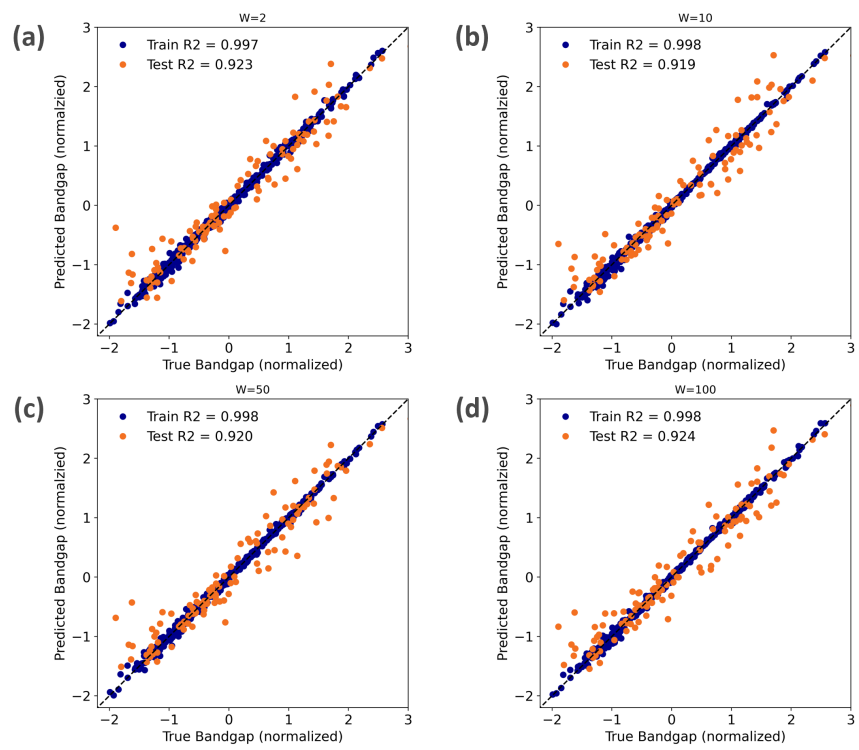


**Figure 10.** SGD training results for language modeling with different regressor head widths,  $W$ : (a)  $W=2$ ; (b)  $W=10$ ; (c)  $W=50$ ; (d)  $W=100$ . Test  $R^2 > 0.9$  (orange points) for all four regressor head we tested, suggesting this is a regression task that can be well-learned by neural networks.